The implications of the surprising existence of a large, massive CO disk in a distant protocluster

Dannerbauer, H.; Lehnert, M.D.; Emonts, B.; Ziegler, B.; Altieri, B.; De Breuck, C.; ... ; Wylezalek, D.

Version:	Not Applicable (or Unknown)
License:	
Downloaded from:	

Astronomy & Astrophysics

The implications of the surprising existence of a large, massive CO disk in a distant protocluster[*]

H. Dannerbauer[1,2,3], M. D. Lehnert[4], B. Emonts[5,6], B. Ziegler[3], B. Altieri[7], C. De Breuck[8], N. Hatch[9], T. Kodama[10], Y. Koyama[10,11], J. D. Kurk[12], T. Matiz[3], G. Miley[13], D. Narayanan[14], R. P. Norris[15,16], R. Overzier[17], H. J. A. Röttgering[13], M. Sargent[18], N. Seymour[19], M. Tanaka[10], I. Valtchanov[7], and D. Wylezalek[20]

[1] Instituto de Astrofísica de Canarias (IAC), 38205 La Laguna, Tenerife, Spain
e-mail: helmut@iac.es
[2] Universidad de La Laguna, Dpto. Astrofísica, 38206 La Laguna, Tenerife, Spain
[3] Universität Wien, Institut für Astrophysik, Türkenschanzstraße 17, 1180 Vienna, Austria
[4] Sorbonne Universités, UPMC Univ. Paris 6 et CNRS, UMR 7095, Institut d'Astrophysique de Paris, 98bis Bd Arago, 75014 Paris, France
[5] Centro de Astrobiología (INTA-CSIC), Ctra de Torrejón a Ajalvir, km 4, 28850 Torrejón de Ardoz, Madrid, Spain
[6] National Radio Astronomy Observatory, 520 Edgemont Road, Charlottesville, VA 22903, USA
[7] Herschel Science Centre, European Space Astronomy Centre, ESA, 28691 Villanueva de la Cañada, Spain
[8] European Southern Observatory, Karl-Schwarzschild-Straße 2, 85748 Garching, Germany
[9] School of Physics and Astronomy, University of Nottingham, University Park, Nottingham NG7 2RD, UK
[10] Optical and Infrared Astronomy Division, National Astronomical Observatory of Japan, Mitaka, 181-8588 Tokyo, Japan
[11] Department of Space Astronomy and Astrophysics, Institute of Space and Astronautical Science (ISAS), Japan Aerospace Exploration Agency (JAXA), 3-1-1 Yoshinodai, Chuo-ku, Sagamihara, 252-5210 Kanagawa, Japan
[12] Max-Planck-Institut für extraterrestrische Physik, Giessenbachstraße 1, 85748 Garching, Germany
[13] Leiden Observatory, PO Box 9513, 2300 RA Leiden, The Netherlands
[14] University of Florida, Department of Astronomy, 211 Bryant Space Sciences Center, Gainesville, FL 32611-2055, USA
[15] CSIRO Astronomy & Space Science, PO Box 76, Epping, NSW 1710, Australia
[16] Western Sydney University, Locked Bag 1797, Penrith South, NSW 1797, Australia
[17] Observatório Nacional, Rua José Cristino 77, 20921-400 São Cristóvão, Rio de Janeiro, Brazil
[18] Astronomy Centre, Department of Physics and Astronomy, University of Sussex, Brighton BN1 9QH, UK
[19] International Center for Radio Astronomy Research, Curtin University, GPO Box U1987, Perth, WA 6845, Australia
[20] Johns Hopkins University Bloomberg Center, Department of Physics & Astronomy, 3400 N. Charles Street, Baltimore, MD 21218, USA

ABSTRACT

It is not yet known if the properties of molecular gas in distant protocluster galaxies are significantly affected by their environment as galaxies are in local clusters. Through a deep, 64 h of effective on-source integration with the Australian Telescope Compact Array (ATCA), we discovered a massive, $M_{\rm mol} = 2.0 \pm 0.2 \times 10^{11}$ $M_\odot$, extended, ~40 kpc, CO(1–0)-emitting disk in the protocluster surrounding the radio galaxy, MRC 1138−262. The galaxy, at $z_{\rm CO} = 2.1478$, is a clumpy, massive disk galaxy, $M_* \sim 5 \times 10^{11}$ $M_\odot$, which lies 250 kpc in projection from MRC 1138−262 and is a known Hα emitter, named HAE229. This source has a molecular gas fraction of ~30%. The CO emission has a kinematic gradient along its major axis, centered on the highest surface brightness rest-frame optical emission, consistent with HAE229 being a rotating disk. Surprisingly, a significant fraction of the CO emission lies outside of the UV/optical emission. In spite of this, HAE229 follows the same relation between star-formation rate and molecular gas mass as normal field galaxies. HAE229 is the first CO(1–0) detection of an ordinary, star-forming galaxy in a protocluster. We compare a sample of cluster members at $z > 0.4$ that are detected in low-order CO transitions, with a similar sample of sources drawn from the field. We confirm findings that the CO-luminosity and full-width at half maximum are correlated in starbursts and show that this relation is valid for normal high-z galaxies as well as for those in overdensities. We do not find a clear dichotomy in the integrated Schmidt-Kennicutt relation for protocluster and field galaxies. Our results suggest that environment does not have an impact on the "star-formation efficiency" or the molecular gas content of high-redshift galaxies. Not finding any environmental dependence in these characteristics, especially for such an extended CO disk, suggests that environmentally-specific processes such as ram pressure stripping do not operate efficiently in (proto)clusters.

Key words. galaxies: clusters: individual: MRC 1138–262 – galaxies: high-redshift – galaxies: evolution – galaxies: ISM – submillimeter: galaxies – galaxies: individual: HAE229

---

1. Introduction

Over the last decade detections of molecular line emission in high-redshift galaxies have become routine (e.g.,

Carilli & Walter 2013). These detections mainly came from observations of the bright high order transitions of CO and generally from extreme source populations such as submillimeter galaxies (SMGs; see Blain et al. 2002; Casey et al. 2014, for detailed reviews) or high-z QSOs (e.g., Walter et al. 2004) which are intrinsically gas-rich ($M_{H_2} \sim$ few times 10^{10} $M_\odot$), or from strongly lensed sources (e.g., Baker et al. 2004; Lestrade et al. 2010; Weiß et al. 2013; Spilker et al. 2014, 2015; Cañameras et al. 2015; Dye et al. 2015; Swinbank et al. 2015; Aravena et al. 2016; Béthermin et al. 2016; Harrington et al. 2016; Sharon et al. 2016). Very few detections are available for normal star-forming galaxies (e.g., Daddi et al. 2008, 2010a, 2014; Dannerbauer et al. 2009; Tacconi et al. 2010, 2013; Genzel et al. 2015). These are found to have substantial reservoirs of molecular gas, but convert their gas into stars with a lower efficiency.

The number of CO detections of galaxies which lie in overdensities (protoclusters) at $z > 1$ is still small (e.g., Daddi et al. 2009; Capak et al. 2011; Aravena et al. 2012; Wagg et al. 2012; Casey 2016; Wang et al. 2016). This is unfortunate and the limited sample size of well-studied protocluster galaxies in CO hampers our ability to study the build-up of galaxy populations in clusters. Almost all of the CO detections of protocluster galaxies are in the environments of high-redshift radio galaxies (Ivison et al. 2008, 2012; Casasola et al. 2013; Emonts et al. 2014). Tadaki et al. (2014) detected three galaxies – two robustly and one tentatively – in CO(1–0) in the protocluster surrounding USS 1558−003 at $z = 2.53$. These three galaxies were all originally identified as Hα emitters (HAEs). They conclude that these HAEs, based on their estimated star-formation efficiencies, $SFE = SFR/M_{mol}$ (the ratio of star-formation rate and molecular gas mass), are gas-rich major mergers. Geach et al. (2011) and Aravena et al. (2012) find that the SFE of IR-bright cluster members are similar to disk-like galaxies at lower redshifts. On the contrary, Ivison et al. (2013) find that two of four discovered CO-bright galaxies within a region of ∼100 kpc do have high SFEs. Jablonka et al. (2013) made the first detailed study of how molecular gas properties depend on the environment beyond the local universe. They find that, at intermediate redshifts, $z \sim 0.4$, environment starts to affect the cold gas content of the most massive galaxies in clusters. Since we know that cluster galaxies in the nearby universe and at moderate redshifts are relatively gas poor (Chamaraux et al. 1980, 1986; Vollmer et al. 2001a; Jablonka et al. 2013), the crucial question to investigate is: When does environment begin to play a significant role in shaping the gas content of galaxies (Vollmer et al. 2001b; Gnedin 2003a,b; Husband et al. 2016)? Of course, like many questions in astrophysics, answering this is hampered by small sample sizes and the lack of systematic studies (cf. Chapman et al. 2015).

In one of the best studied protocluster fields, MRC 1138−262 at $z = 2.16$ (e.g., Kurk et al. 2000, 2004a,b; Pentericci et al. 2000; Hatch et al. 2011; Dannerbauer et al. 2014; Emonts et al. 2016), using the Australia Telescope Compact Array (ATCA), Emonts et al. (2013) tentatively detected the CO(1–0) emission from the Hα bright galaxy, HAE229 (Kurk et al. 2004b; Doherty et al. 2010). Dannerbauer et al. (2014) found evidence that HAE229 – about 30″ (∼250 kpc in projected distance) from the radio galaxy MRC 1138−262 – is an SMG and part of the overdensity of dusty starbursts in the field of MRC 1138−262. Its redshift also indicates it is a protocluster member (Kuiper et al. 2011). Here we present a robust detection of the CO(1–0) line of this source adding new, deeper, and higher-resolution ATCA data (Emonts et al. 2013). Other than the radio galaxy MRC 1138−262 (Emonts et al. 2013, 2016), HAE229 is the first

unambiguously confirmed gas-rich member of this well-studied protocluster.

The structure of this paper is as follows. Sections 2 and 3 describe the properties of HAE229 and our new ATCA observations. In Sect. 4 we present the results of the CO(1–0) observations of HAE229 and in Sect. 5 we discuss the properties of this gas-rich HAE and compare the molecular gas properties of protocluster galaxies and field galaxies. We adopt the cosmological parameters $\Omega_m = 0.27$, $\Omega_\Lambda = 0.73$, and $H_0 = 71$ km s^{-1} Mpc^{-1} (Spergel et al. 2003, 2007). At redshift $z = 2.16$, 1 arcsec corresponds to 8.4 kpc. All magnitudes in this paper are on the AB magnitude scale (Oke & Gunn 1983) and we assume a Salpeter initial mass function (IMF; Salpeter 1955) in our analysis.

2. A brief history of HAE229

Kurk et al. (2004a) discovered HAE229 through Hα narrow-band imaging at the approximate redshift of the radio galaxy. The excess emission in the narrow-band image of HAE229 was subsequently confirmed spectroscopically to be Hα emission at $z = 2.1489$ (Kurk et al. 2004b; see also Koyama et al. 2013). Doherty et al. (2010) found that HAE229 (#464 in their paper) is a massive, dust-obscured star-forming red galaxy, $[J-K] > 2.41$, with a stellar mass, $M_* = 5.1^{+1.5}_{-2.0} \times 10^{11}$ $M_\odot$, and a star-formation rate estimated from spectral energy distribution (SED) fitting, $SFR_{SED} = 35 \pm 6$ $M_\odot$ yr^{-1}. Ogle et al. (2012) observed this source with *Spitzer IRS*, detecting polycyclic aromatic hydrocarbons (PAH) emission at 7.7 μm, concluding that the star formation in HAE229 is heavily obscured and implying a much higher SFR, $SFR_{PAH} = 880$ $M_\odot$ yr^{-1}, than was estimated previously (e.g., Doherty et al. 2010). HAE229 is one of the most massive HAEs embedded in the large scale structure at $z = 2.16$ (see Fig. 6 in Koyama et al. 2013; and Fig. 8 in Dannerbauer et al. 2014). Finally, when observing the radio galaxy MRC 1138−262 with ATCA, Emonts et al. (2013) serendipitously found a tentative CO(1–0) emission line at $z_{CO} = 2.147$ at the position of HAE229 and Dannerbauer et al. (2014) associated this source with a Submillimeter Common-User Bolometric Array (SCUBA) submm detection (Stevens et al. 2003).

3. Observations

3.1. ATCA observations of CO(1–0)

Our CO(1–0) observations of HAE229 were performed with the Australia Telescope Compact Array during April 2011–February 2015 in the H75, H168, H214, 750A, 750D, and 1.5A array configurations and only including baselines ranging from 31−800 m in our reduction. Data from the longest baselines of the 1.5A array configuration were discarded because these data were obtained during day-time under moderate weather conditions. Excluding them from the reduction resulted in a more uniform uv-coverage and a more robust image. Our total on-source integration time is ∼90 h. Our primary goal with these observations was to obtain ultra-deep data on the radio galaxy within the protocluster MRC 1138−262. Hence the pointing center of the observations was 30 arcsec east of our target HAE229 (see Emonts et al. 2013). This increased the effective noise at its location by a factor of ∼1.4 as a result of the primary beam correction ($FWHM_{PrimBeam} \sim 77$ arcsec). The effective integration time is therefore only 60 h or 2/3rd of the total on-source time. Observations were centered around 36.5 GHz, using a channel width of 1 MHz and an effective bandwidth of 2 GHz.

Phase and bandpass calibration were performed by observing the strong calibrator PKS 1124−186 every 5−12 min. The frequency of the observations depended on the weather conditions. However, given the 8.2° distance of PKS 1124–186 from our target, we used the weaker but closer (2.8°) calibrator PKS 1143–287 for phase calibration in the more extended 750A/D and 1.5A array configurations. The bandpass calibration scans of PKS 1124–186 were taken approximately every hour. An absolute flux scale was determined using observations of Mars for array configurations, H75 and H168, the ultra-compact H II region G309 for H214, and PKS 1934–638 for array configurations, 750A/D and 1.5A (Emonts et al. 2011)[1]. The strong radio continuum of MRC 1138−262 allowed us to verify that the flux scaling between all observations stayed within the typical 30% accuracy for flux calibration at the ATCA. These data were reduced in MIRIAD (Sault et al. 1995) and analysed with the KARMA software (Gooch 1996), following the strategy described in Emonts et al. (2013). The continuum-subtracted line-data products that we present in this paper were weighted using a robustness parameter of +1 (Briggs 1995), binned into 34 km s^{-1} channels and subsequently Hanning-smoothed to an effective velocity resolution of 68 km s^{-1} (equivalent to two 34 km s^{-1} binned channels). This procedure results in a root-mean-square noise of 0.12 mJy beam^{-1} per channel in the region of HAE229, after correcting for the primary beam response. At the half-power point, the synthesized beam is 4″.7 × 3″.1 (PA = −6°). Velocities in this paper are defined in the optical barycentric reference frame with respect to $z = 2.1478$.

3.2. HAWK-I

We mapped the field around the radio galaxy, MRC 1138−262, with the near-infrared wide-field imager High Acuity Wide field K-band Imager (HAWK-I) at the ESO Very Large Telescope (VLT). The observations were taken in the Y-, H-, and K_s-bands during February and March 2012, April, May, and July 2013, and January and February 2015 in service mode. The seeing was 0″.4−0″.6 during these observations. The dithered HAWK-I data were reduced using the ESO/MVM data reduction pipeline (Vandame 2004), following the standard reduction steps for near-infrared imaging data.

4. Results

HAE229 has been observed with the Advanced Camera for Surveys (ACS) on *Hubble* Space Telescope (HST) through the *F475W* and *F814W* filters (Miley et al. 2006) and with the Near Infrared Camera and Multi-Object Spectrometer (NIC-MOS) on HST through the J_{110} and H_{160} filters (Zirm et al. 2008). In all of these images, we only detect HAE229 in the ACS *F814W* band (rest-frame ∼2560 Å)[2]. There are several regions of higher surface brightness rest-frame UV emission seen in the HST image (labeled a, b, c, d; Fig. 1) embedded in more diffuse, lower surface brightness emission. Two of them, a and b, are "clumps" of UV emission (meaning marginally extended, point-like sources), while c and d have fainter clumps
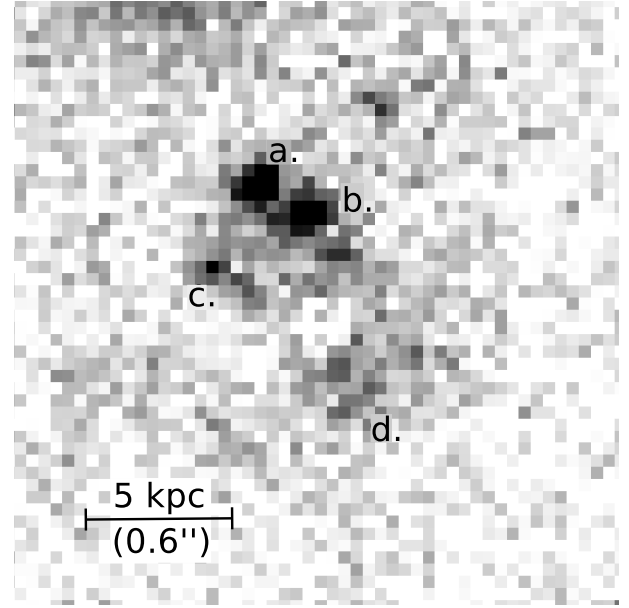
---

[1] The reason for altering the flux calibrators is that the reliability of the absolute flux scale of PKS 1934–638 was still questionable during the epoch 2011–2013. Mars was not always visible and G309 (with flux bootstrapped from Uranus; Emonts et al. 2011) is fully resolved in the longer-baseline 750A/D and 1.5A array configurations.

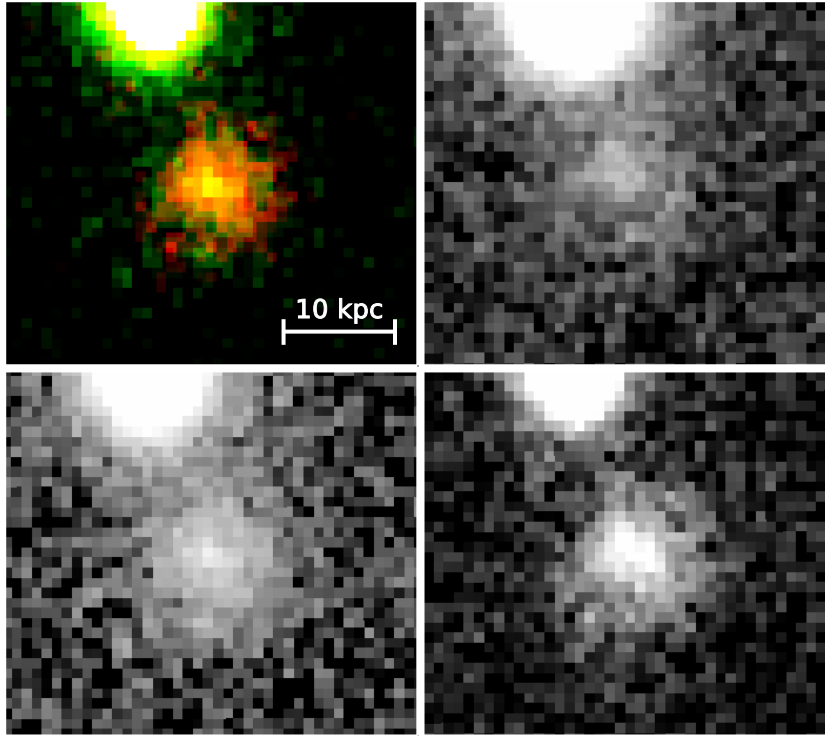[2] We note that Koyama et al. (2013) discuss the HST *F814W* imaging of 54 HAEs, one of which is HAE229.

Fig. 1. The 3″ × 3″ HST *F814W* image of the clumpy galaxy, HAE229. The size of HAE229 is 1″.2 × 0″.6 (10 × 5 kpc). Regions a and b are clumpy and knot-like whereas areas c and d have more diffuse rest-frame UV emission morphology.

superposed on diffuse continuum emission. The size of this clumpy galaxy – with marginally resolved sources evident in the HST/ACS light distribution system – is 1″.2 × 0″.6 (10 × 5 kpc). Despite its clumpy structure, estimating the "Gini" coefficient (e.g., Abraham et al. 2003) of the HST *F814W* image of HAE229 suggests that its light is dominated by a uniform, lower surface brightness diffuse component (see Koyama et al. 2013, for details). We detect this source in Subaru MOIRCS and VLT HAWK-I near-infrared imagery but not in shallower HST near-infrared (NIR) images. At near-infrared wavelengths, HAE229 becomes much more regular in appearance (Fig. 2). We do not see an offset of centers between the rest-frame UV (∼2560 Å) and rest-frame optical regions (∼3063−7300 Å) of HAE229. The comparable images of normal SFGs (star-forming galaxies) shows that they often consist of clumps within diffuse continuum emission similar to what we observe for HAE229 (see the image montages in, e.g., Tacconi et al. 2013). In addition, the highest surface brightness region in the near-infrared, presumably the center of mass of the stellar component, is very red and is responsible for giving HAE229 its overall red color. Again, this is found among many distant disk galaxies, especially ones that are similarly massive (e.g., Pannella et al. 2009)

The CO(1−0) transition is now robustly detected in our new data for HAE229, with a total significance of ∼7σ (Fig. 3). We measure a peak flux, $S_v = 0.57 \pm 0.06$ mJy beam^{-1}, at the position: RA$_{2000.0}$ = 11:40:46.05 and Dec$_{2000.0}$ = −26:29:11.2s (Table 1). The full-width at half maximum (FWHM) of the line is 359 ± 34 km s^{-1} and we obtain an integrated flux, $I_{CO(1−0)} = 0.22 \pm 0.03$ Jy km s^{-1}. The CO line redshift $z_{CO(1−0)} = 2.1478 \pm 0.0002$ agrees with the redshift estimate obtained using Hα (Kurk et al. 2004b; Doherty et al. 2010). Both the measured redshift and line FWHM are consistent with the results of Emonts et al. (2013) for their tentative detection. However, the flux density increased by 80%. We derive $L'_{CO(1−0)} = 5.0 \pm 0.07 \times 10^{10}$ K km s^{-1} pc^2 from the current data set. We stress that the uncertainties in the flux and luminosity estimates are

Fig. 2. The $4.2'' \times 3.7''$ regions centered on HAE229. *Top left panel*: a composite three-color image made by combining the Y-, H-, and K_s-band color images taken with HAWK-I on the ESO/VLT (see text and Table 2 for details). To show the rest-frame blue and red optical morphology, we show each color component of the composite separately, namely, Y-band (approximately rest-frame U-band, *top right*), H-band (approximately rest-frame B- or V-band, *bottom left*) and K_s-band (approximately rest-frame R-band, *bottom right*). The Y-band image has a morphology similar to that of the *F814W* image and no offset is detected between the rest-frame UV and rest-frame optical regions. With increasing wavelength, the emission becomes less clumpy, more regular, and a red nucleus is evident. The dynamical center of the CO(1–0) emission corresponds to the highest surface brightness region of the H- and K_s-band images suggesting this region is also the center of mass of the galaxy. The bright galaxy above HAE229 in all panels lies at $z_{\rm phot} \approx 0.5$ (Tanaka et al. 2010).
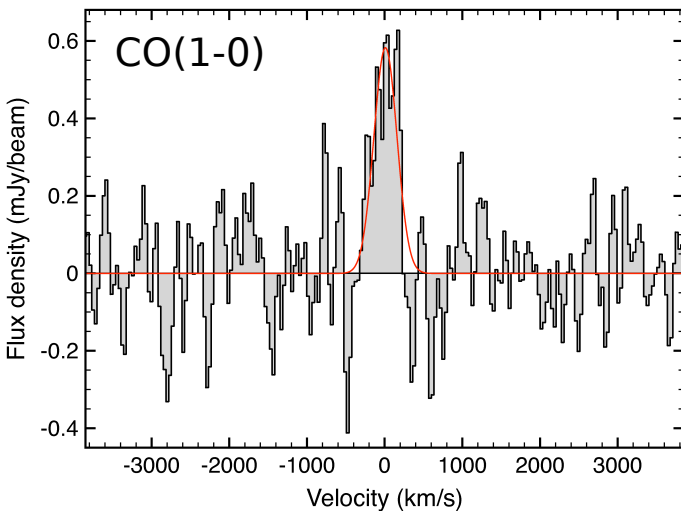

Fig. 3. CO(1–0) spectrum of HAE229 from data taken with the compact hybrid ATCA configurations (for which the signal is spatially unresolved). The red line shows a Gaussian fit from which we derived z, $L'_{\rm CO(1-0)}$ and FWHM$_{\rm CO(1-0)}$.

measurement errors, and do not include the 30% uncertainty in absolute flux calibration (Sect. 3.1), or potential errors in the primary beam calibration (which may be important considering

that HAE229 is located close to the edge of the primary beam; Sect. 3.1).

The most important new finding in these deeper data is that the emission in HAE229 appears to be very extended and is rotating about the center of mass as indicated in our near-infrared imaging (Fig. 4). The northwestern and southeastern sides of the rotating disk are separated ~1.8″ or about ~15 kpc in projection, along PA ~ −22°. Their midpoint corresponds to the peak surface brightness of the continuum emission in the near-infrared (within the uncertainties in the astrometry of each data set; Fig. 4). The position-velocity diagram along the blue and the red velocity components on the northeastern and southwestern sides of the disk (Fig. 4) shows a velocity gradient of ~200 km s^{-1} in projection. The most likely explanation for the gas properties is rotation of a gaseous disk around the center of the stellar mass of the system. The total CO emission is spread over a region of ≈40 kpc in diameter and much of the gas is well outside the lowest surface brightness stellar continuum emission detected in the optical and near-infrared imaging.

In Fig. 5, we show the rest-frame UV through the FIR/submm spectral energy distribution (SED) of HAE229 (Table 2). We compared the SED of HAE229 with those from a variety of other sources (see Pope et al. 2008; Weiß et al. 2009; Michałowski et al. 2010; Magdis et al. 2012; Hodge et al. 2013b; Karim et al. 2013; Swinbank et al. 2014). The far-infrared SED of HAE229 is similar to the templates which we have chosen for making our comparison. The template of the main-sequence galaxies resembles most closely the far-infrared

Table 1. Positions of HAE229.

ID	Instrument	RA (J2000.0)	Dec (J2000.0)	Offset ΔCO − Other	Reference
CO counterpart	ATCA	11:40:46.05 ± 0.05	−26:29:11.2 ± 0.6	−	this paper
HAE#229	VLT-ISAAC	11:40:46.1	−26:29:11.5	0.7	Kurk et al. (2004a)
HAE#902	Subaru-MOIRCS	11:40:46.065	−26:29:11.33	0.2	Koyama et al. (2013)

Notes. Units of right ascension are hours, minutes, and seconds, and units of declination are degrees, arcminutes, and arcseconds.
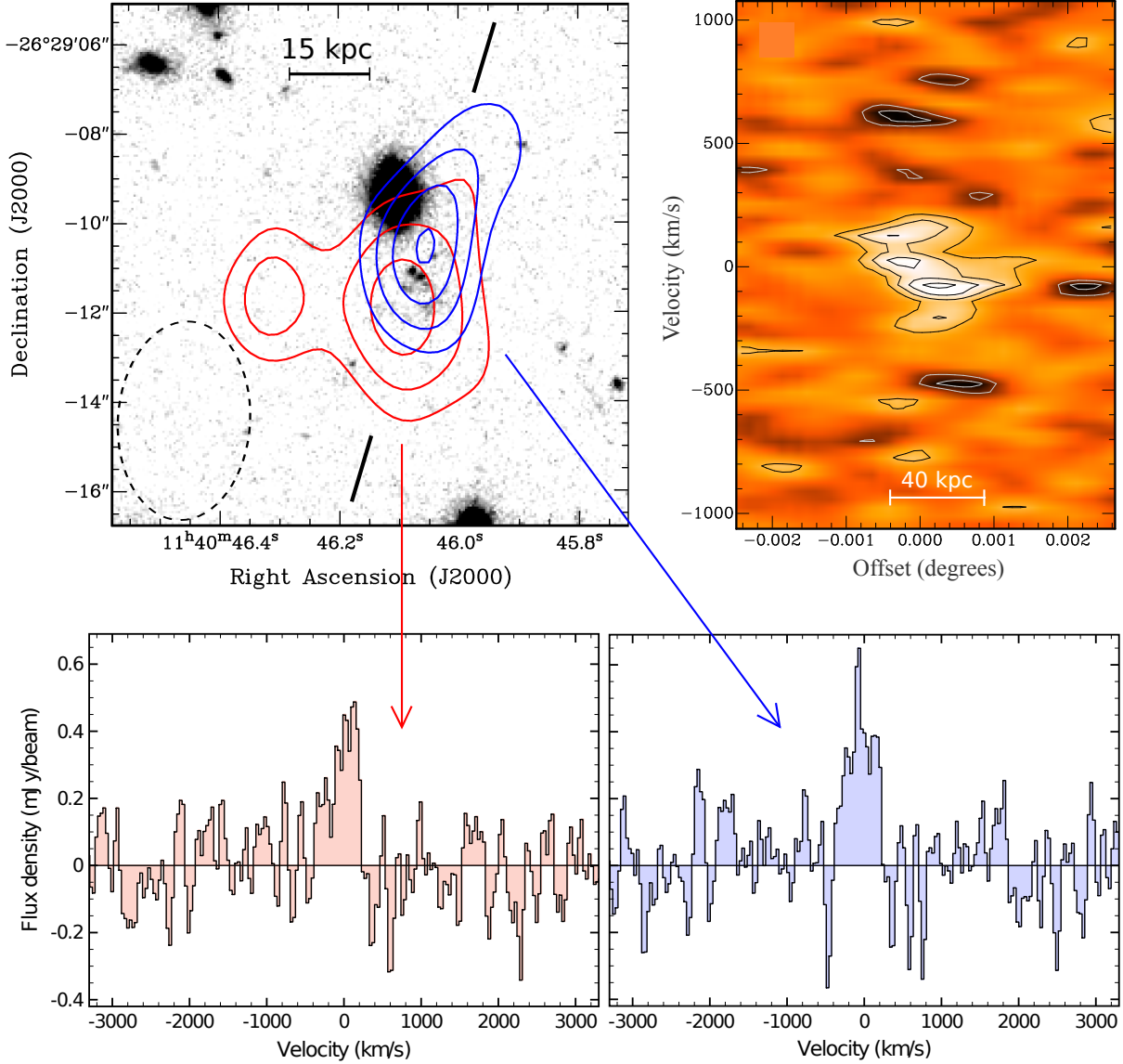

Fig. 4. Overview of the CO(1–0) full-resolution ATCA data. *Top left*: total intensity image of the CO(1–0) emission across the velocity ranges $-200 < v < 0$ km s^{-1} (blue contours) and $0 < v < +200$ km s^{-1} (red contours). Contour levels are 3, 4, 5, 6σ, and $\sigma = 0.015$ Jy beam^{-1} km s^{-1}. Following Papadopoulos et al. (2008), the relative accuracy in the position of the CO peak emission is $\lesssim 0.4''$. The dashed circle indicates the half-power size of the synthesized beam. *Top right*: position-velocity plot of the CO(1–0) emission along the line indicated in the top-left plot (along the northwestern-southeastern direction). Contours level shown are −4, −3, −2 (gray), 2, 3, 4, 5 (black) σ. *Bottom*: CO(1–0) spectra of the peak emission in the blue- and red-shifted velocity components as indicated in the plot at the top left. The spectra are not mutually independent due to the relatively large beam and due to having velocities that over-lap.

SED of HAE229. Just like another protocluster galaxy, DRG55 (Chapman et al. 2015), HAE229 is significantly fainter at rest-frame wavelengths $\lesssim 1\,\mu$m, demonstrating that it is extremely red and is highly dust-enshrouded. We note that redshifted, $z = 2.2$ [CII]158 μm emission contributes to the SPIRE 500 μm flux (see also Smail et al. 2011, for a more detailed discussion of this effect). The uncertainty in the SCUBA submm flux measurements of this source is evident in the offset of the different templates relative to these measurements (Stevens et al. 2003). The SED of HAE229 appears to be typical of the general population of

dusty star-forming galaxies in the infrared and submm. By integrating the infrared emission from $40-1000$ μm, we estimate a star-formation rate of $SFR_{IR} = 555$ $M_\odot$ yr^{-1} for HAE229[3].

5. Discussion

In extremely deep observations with the ATCA, we have found a very extended, massive, rotating disk of cold gas in a galaxy embedded in the protocluster surrounding the radio galaxy, MRC 1138−262. HAE229 has a high stellar mass, a few 10^{11} $M_\odot$, already in place at $z = 2.16$. Its high CO(1–0) luminosity suggests that it has a similar mass in cold molecular gas. HAE229 is moving at high speed relative to the radio galaxy MRC 1138−262, over −1200 km s^{-1}, and has a small projected separation, ∼250 kpc (Emonts et al. 2013). Dannerbauer et al. (2014) showed that the far-IR and sub-mm emission detected by *Herschel*/SPIRE 250 μm and APEX LABOCA at the position of MRC 1138−262 is extended in the direction of HAE229. Although it has a relatively high velocity relative to the radio galaxy, it has a similar velocity to other protocluster galaxies that lie to the west of the radio galaxy (Kuiper et al. 2011), so it is likely that HAE229 is a member of the protocluster surrounding MRC 1138−262.

HAE229 is the first CO(1–0) emitting HAE that is classified as a disk galaxy in a (proto)cluster. This is only the fifth detection of CO in an HAE residing in an overdensity at high redshift. For all, with one exception, DRG55 (Chapman et al. 2015), the low-order CO transitions are detected, enabling robust estimates of their total molecular gas mass to be made without significant uncertainties due to the unknown excitation of the gas. Three galaxies with possible low-order CO detections, bHAE-191, rHAE-193, and rHAE-213 (which is only tentatively detected), reside in the protocluster USS 1558−003 at $z = 2.53$ (Tadaki et al. 2014) and two of them[4], bHAE-191 and rHAE-193, are classified as mergers.

Given the uniqueness of HAE229 – it has a large content of molecular gas and very extended molecular emission – there are several interesting questions to address. What is the nature of this galaxy? Given that its stellar mass is already very high, that the co-moving space density of star-forming galaxies this massive is extremely low ($\lesssim10^{-5.5}$ Mpc^{-3}; Ilbert et al. 2013), and that the galaxy is also gas-rich, what processes might prevent it from further increasing its stellar mass substantially? Does its location in a protocluster at high redshift affect any of the properties of its cold gas or the nature of its star formation? Do galaxies in protoclusters form their stars as efficiently as field galaxies? Are their gas fractions significantly lower than those in nearby cluster galaxies? We now address these questions.

5.1. The nature of HAE229

A key aspect of understanding the nature of distant galaxies is determining their mode of star formation (Daddi et al. 2010b; Genzel et al. 2010; Narayanan et al. 2015). Distant galaxies are hypothesized to have two modes of star formation, a "quiescent mode" and a "starburst mode". The quiescent mode refers to galaxies having relatively long gas depletion timescales ($t_{dep} \equiv M_{H_2}/SFR$, where M_{H_2} is the mass of molecular gas and SFR is

---

[3] We note that if we used a Chabrier stellar initial mass function (Chabrier 2003) instead of a Salpeter IMF, our estimated SFR_{IR} would be a factor of 1.8 smaller.
[4] The third source, rHAE-213, has no reliable FIR-measurements.
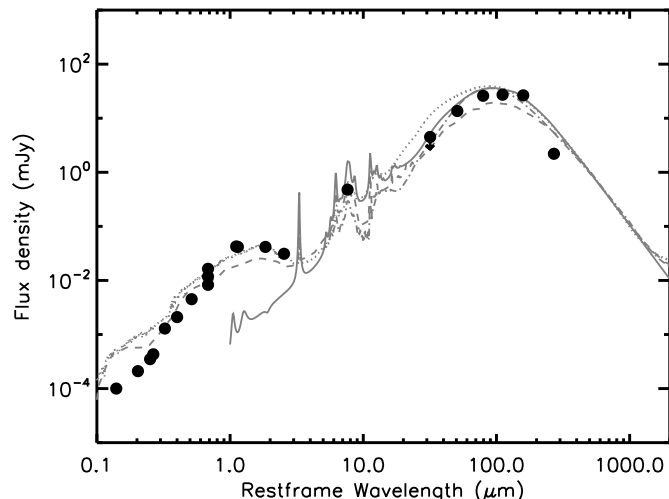
Fig. 5. Spectral energy distribution of HAE229 (black filled circles). We show the template SED (solid line) of a main-sequence galaxy at $z = 2$ (Magdis et al. 2012) which is based on models (Draine & Li 2007). In addition, template SEDs of observed SMGs are shown for comparison: ALESS SMG composite (dotted line – Swinbank et al. 2014), average SED of 73 spectroscopically identified SMGs (dashed line – Michałowski et al. 2010), and an average SED of SMGs (dashed-dotted line – Pope et al. 2008). The far-infrared SED is matched by the different SMG composites whereas the rest-frame optical SED shows that HAE229 is redder than the average of various types of dusty vigorously star-forming galaxies at high redshift.

the star-formation rate) of $0.5-2$ Gyr (e.g., Leroy et al. 2008; Bigiel et al. 2008; Daddi et al. 2010b; Tacconi et al. 2013). This mode has been hypothesized to be due to the long dynamical times of disk galaxies. Galaxies in "starburst" mode have short gas depletion times, $\lesssim100$ Myr (e.g., Greve et al. 2005; Ivison et al. 2011), and complex morphologies and dynamics. This mode is hypothesized to be triggered by major mergers of two or more gas-rich disk galaxies.

In distant, $z \sim 2$ protoclusters, cold molecular gas reservoirs have only been detected in starbursts (Hodge et al. 2012, 2013a; Ivison et al. 2013; Riechers et al. 2010; Tadaki et al. 2014; Walter et al. 2012). Chapman et al. (2015) report the blind detection of star-forming molecular gas via the CO(3−2) transition of the extremely red, main sequence galaxy DRG55 in the protocluster HS1700+64. The equivalent width of the Hα emission of this source is high suggesting that it has formed a substantial fraction of its stellar mass relatively recently (Chapman et al. 2015). Another four UV-selected main-sequence SFGs in HS1700+64 are detected in CO(3−2) (Tacconi et al. 2013). Detecting low excitation CO lines of normal, star-forming galaxies in overdensities is rare. This is predominately due to the lack of systematic, targeted low-J CO studies of galaxies in overdensities. Very recently Wang et al. (2016) reported the detection of 11 galaxies in CO(1−0) in a cluster at $z = 2.51$. HAE229 has an exquisite multi-wavelength data set available which enables us to investigate this galaxy in detail (see Table 2 and Fig. 5). From these data, there are extensive estimates of the properties of HAE229 such as luminosities, masses, and (specific) star-formation rates (Table 3).

5.1.1. The molecular gas in HAE229

How gas-rich is HAE229 actually? This is difficult to estimate accurately due to the significant uncertainties in determining the CO luminosity to molecular gas-mass conversion

Table 2. Fluxes of HAE229.

Band	Unit	HAE229	Instruments	Reference
(1)	(2)	(3)	(4)	(5)
B	mag	26.36 ± 0.68	FORS2	Koyama et al. (2013)
Y	mag	23.62 ± 0.32	HAWK-I	this paper
J	mag	23.09 ± 0.03	MOIRCS	Koyama et al. (2013)
H	mag	22.26 ± 0.10	HAWK-I	this paper
$K_{\rm s}$	mag	21.22 ± 0.08	HAWK-I	this paper
$K_{\rm s}$	mag	20.86 ± 0.09	MOIRCS	Doherty et al. (2010)
$K_{\rm s}$	mag	21.60 ± 0.02	MOIRCS	Koyama et al. (2013)
$S_{3.6\ \mu m}$	mag	19.85 ± 0.1	IRAC	this paper
$S_{4.5\ \mu m}$	mag	19.83 ± 0.1	IRAC	this paper
$S_{5.8\ \mu m}$	mag	19.85 ± 0.2	IRAC	this paper
$S_{8.0\ \mu m}$	mag	20.16 ± 0.2	IRAC	this paper
$S_{24.0\ \mu m}$	μJy	477.4 ± 5.0	MIPS	Dannerbauer et al. (2014)
$S_{100\ \mu m}$	mJy	<4.5	PACS	Dannerbauer et al. (2014)
$S_{160\ \mu m}$	mJy	13.6 ± 4.0	PACS	Dannerbauer et al. (2014)
$S_{250\ \mu m}$	mJy	26.0 ± 2.8	SPIRE	Dannerbauer et al. (2014)
$S_{350\ \mu m}$	mJy	27.2 ± 2.9	SPIRE	Dannerbauer et al. (2014)
$S_{500\ \mu m}$	mJy	26.5 ± 2.7	SPIRE	Dannerbauer et al. (2014)
$S_{850\ \mu m}$	mJy	2.2 ± 1.4	SCUBA	Stevens et al. (2003)
$S_{\rm CO(1-0)}$	mJy	0.57 ± 0.06	ATCA	this paper
$I_{\rm CO(1-0)}$	Jy km s^{-1}	0.22 ± 0.03	ATCA	this paper

Table 3. Properties of HAE229.

Property	HAE229	Reference
$z_{\rm CO(1-0)}$	2.1478 ± 0.0002	this paper
$z_{\rm H\alpha}$	2.1489	Kurk et al. (2004b)
$z_{\rm H\alpha}$	2.149	Doherty et al. (2010)
$FWHM$ of CO(1−0)	359 ± 34 km s^{-1}	this paper
$FWHM$ of Hα	290 ± 60 km s^{-1}	Kurk et al. (2004b)
$L'_{\rm CO(1-0)}$	$5.0 \pm 0.7 \times 10^{10}$ K km s^{-1} pc^2	this paper
$L_{\rm IR}$	$3.2 \times 10^{12}\ L_\odot$	this paper
SFE	$66\ L_\odot$ K km s^{-1} pc^2	this paper
$SFR_{\rm PAH}$	$880\ M_\odot$ yr^{-1}	Ogle et al. (2012)
$SFR_{\rm IR}$	$555\ M_\odot$ yr^{-1}	this paper
$SFR_{\rm H\alpha}$	$389\ M_\odot$ yr^{-1}	Koyama et al. (2013)
$SFR_{\rm SED}$	$35 \pm 6\ M_\odot$ yr^{-1}	Doherty et al. (2010)
$M_\star$	$3.7 \times 10^{11}\ M_\odot$	Koyama et al. (2013)
$M_\star$	$5.1^{+1.5}_{-2.0} \times 10^{11}\ M_\odot$	Doherty et al. (2010)
$M_{\rm dust}$	$3.5 \times 10^8\ M_\odot$	this paper
$M_{\rm gas}$	$1.8 \pm 0.2 \times 10^{11}\ M_\odot$	this paper
$12 + \log({\rm O/H})$	8.8	this paper
$\alpha_{\rm CO(1-0)}$	$4.0\ M_\odot$ pc^{-2} (K km s^{-1})$^{-1}$	this paper
sSFR	1.1 Gyr^{-1}	this paper
$M_{\rm gas}/M_\star$	$0.35-0.49$	this paper
$f_{\rm mol}$	$0.27-0.33$	this paper
$t_{\rm dep}$	0.36 Gyr	this paper
$t_{\rm dyn}$	0.12 Gyr	this paper
$t_{\rm SFR}$	$0.67-0.92$ Gyr	this paper

factor. The conversion factor depends on the gas-phase metallicity and complex gas physics (see for a review Bolatto et al. 2013). Ignoring the complexities of determining the appropriate conversion factor, we focus on using its metallicity dependence to constrain the conversion factor for HAE229. Kurk et al. (2004b) find a log [NII]/Hα ratio of −0.47, typical of star-forming galaxies at these redshifts (there is no evidence for a strong Active Galactic Nuclei (AGN) contribution; Ogle et al. 2012; Koyama et al. 2013). The [NII]/Hα ratio implies a metallicity, $12 + \log({\rm O/H}) \approx 8.6-8.8$ (Kurk et al. 2004b; Pettini & Pagel 2004; Denicoló et al. 2002; Mannucci et al. 2010; Maier et al. 2014). We apply the gas-to-dust ratio method, "δGDR", for estimating the CO-to-H$_2$ gas conversion factor,

$\alpha_{\rm CO}$ (Leroy et al. 2011; Magdis et al. 2011, 2012). This method relies on an estimate of the dust mass for which we find $M_{\rm dust} = 3.5 \times 10^9\ M_\odot$ (using the method of Casey 2012). Using the equation $\log \delta{\rm GDR} = (10.54 \pm 1.0) - (0.99 \pm 0.12) \times (12 + \log({\rm O/H}))$ (Magdis et al. 2012), we estimate the CO-to-H$_2$ conversion factor, obtaining, $\alpha_{\rm CO} = 4.7-6.9\ M_\odot$ pc^{-2} (K km s^{-1})$^{-1}$. The range of $\alpha_{\rm CO}$ we give here depends on the method (Denicoló et al. 2002; Pettini & Pagel 2004; Mannucci et al. 2010). Using a metallicity-dependent conversion factor suggests that HAE229 is similar to local and distant normal main-sequence disk galaxies.

Given all of the uncertainties in estimating the conversion factor, it is not entirely clear whether basing an estimate directly
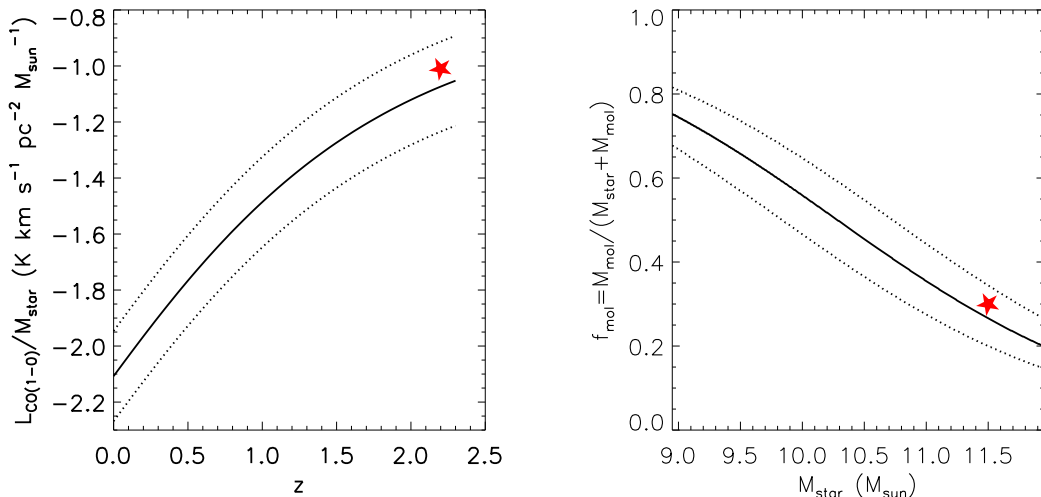
Fig. 6. *Left panel*: ratio of the CO emission and stellar mass in units of K km s^{-1} pc^{-2} $M_\odot^{-1}$ versus redshift. The solid and dotted line shows the median and 1σ dispersion of this ratio for main-sequence galaxies with a mass of 5×10^{11} $M_\odot$. The mass we have chosen for this comparison is approximately the stellar mass of HAE229. *Right panel*: molecular gas fractions and $\pm 1\sigma$ dispersion (solid and dotted lines respectively) for main sequence galaxies at $z = 2.2$. The lines shown in both panels are from models discussed in Sargent et al. (2014) to explain the evolution of the main sequence of galaxies. The red star represents the estimated position of HAE229 in both panels.

on the dust mass and metallicity is completely appropriate or robust. Another way of estimating the conversion factor is to use an independent estimate of the gas mass and simply scale the CO luminosity to give the same gas mass. For example, we can use the empirical calibration of the long wavelength dust continuum emission to estimate the total gas mass (Scoville et al. 2016). Using the 850 μm flux density, we find a total gas mass, $M_{gas} \sim 3 \times 10^{11}$ $M_\odot$. This estimate includes an unconstrained contribution from HI, so this provides only an upper limit to the conversion factor and implies $M_{mol}/L'_{CO(1-0)} \lesssim 6$.

All of our estimates favor a relatively high CO conversion factor. HAE229 has a high infrared luminosity, it is an SMG (although the detection at 850 μm is not highly significant). Many authors favor a low value of the conversion factor for luminous infrared sources (0.8 $M_\odot$ (K km s^{-1} pc^2)$^{-1}$; Solomon & Vanden Bout 2005). With these caveats in mind, we adopt a conversion factor of four (typically for high-z disk-like galaxies, see e.g., Daddi et al. 2010a), implying a total cold molecular gas mass, $M_{mol} = 2.0 \pm 0.2 \times 10^{11}$ $M_\odot$. Adopting a low value generally appropriate for luminous galaxies like HAE229 would lead to conflicts with other estimates of gas masses given previously which do not rely on the conversion factor directly (e.g., Casey 2012; Scoville et al. 2016).

Using the adopted conversion factor and CO luminosity, we estimate a molecular gas fraction, $f_{mol} = M_{mol}/(M_{mol} + M_\star)$, of $\sim$30% for HAE229. In Fig. 6, we show the expected redshift evolution of the ratio between CO luminosity and stellar mass based on the empirical scaling relations for a typical main-sequence galaxy (see Sargent et al. 2014). HAE229 lies well on the predicted relation for main-sequence galaxies at $z = 2.2$. The same applies when comparing HAE229 to the expected average variation of the gas fraction with stellar mass for galaxies at the redshift of HAE229 (Fig. 6).

5.1.2. Timescales: Do the disk dynamics limit star formation in HAE229?

A quantitative way to obtain insights into the "mode of star formation" in galaxies is to derive their specific star-formation rate

and "star-formation efficiency". If HAE229, for its stellar mass and redshift, is a typical main-sequence galaxy, we would expect its star-formation rate, $SFR_{MS} \approx 460$ $M_\odot$ yr^{-1} (Tacconi et al. 2013). We derived a far-infrared based star-formation rate of $SFR_{IR} = 550$ $M_\odot$ yr^{-1} (Sect. 4) which falls within 20% of SFR_{MS} at its redshift, that is, well within the 1-sigma scatter of the relation between SFR and stellar mass (e.g., Magdis et al. 2012). HAE229 is a distant, massive main-sequence galaxy.

Our estimate of the star-formation rate (Sect. 4) and molecular gas mass implies a gas depletion time, $t_{dep} \approx 360$ Myr[5]. The range of star-formation rates that have been estimated for HAE229 implies a systematic uncertainty in the gas depletion time of about a factor of two. Our estimate for HAE229 is similar to the depletion times derived for star-forming galaxies at $z = 1-3$ that are not undergoing a major merger (Daddi et al. 2007; Genzel et al. 2010; Rodighiero et al. 2011), but are up to an order-of-magnitude higher than the typical depletion times derived for SMGs (Greve et al. 2005; Tacconi et al. 2008; Ivison et al. 2011; Riechers et al. 2011), although Swinbank et al. (2006) do consider some exceptions. This is another indication that HAE229 is a normal high-z star-forming galaxy.

The dynamical time (rotational), $t_{dyn} = 2\pi r/(v/\sin i) = 610$ Myr $\times r_{10 kpc}/(v/\sin i)_{100 km s^{-1}}$, where $r_{10 kpc}$ is the radius in units of 10 kpc, $(v/\sin i)_{100 km s^{-1}}$ is the inclination corrected velocity in units of 100 km s^{-1}, and i, is the inclination. In order to constrain the inclination, we estimate the rotation speed needed for the disk to be centrifugally supported, $i \lesssim 30°$, and $(v/\sin i) \approx 500$ km s^{-1}. At 10 kpc, the dynamical time is $\sim$120 Myr. But the gas may be extended over a region up to twice this large and thus, in the case of HAE229, $t_{dep}/t_{dyn} \approx 2-3$. Finding that the gas depletion timescale is a factor of a few greater than the dynamical time is interesting in light of the gas distribution relative to that of the on-going star formation in HAE229. The molecular gas appears to spread over a larger area than the stellar continuum. Thus it is clear that we must consider the role

---

[5] We note that, if we adopt a lower CO-to-molecular gas mass conversion factor, say $\alpha_{CO} = 1$, the gas depletion time for HAE229 would be about 100 Myr (see Casey 2016).

the high angular momentum of the extended disk plays in regulating future star formation. While we do not have the resolution to investigate the detailed kinematics of the disk, the fact that the gas distribution is so extended and has significant angular momentum makes us wonder if it could be that HAE229 will not be able to support its on-going star formation for a gas-depletion timescale, but will use up the gas in the central regions most quickly. In this case, what limits the time over which intense star formation takes place is not when the gas over the disk is exhausted, but how long it takes for the gas to dissipate its angular momentum and to move from the outer to the inner disk. Perhaps it is the high angular momentum of the gas and the rate at which the extended gas in galaxies dissipates angular momentum that ultimately regulates the duration of intense star formation (see Lehnert et al. 2015).

In order to sustain the SFR of HAE229 beyond a dynamical time, $\approx 500~M_{\odot}$ yr^{-1} of gas must be accreted into its central region where the on-going intense star formation is concentrated. While there is a large reservoir of gas in the outskirts to feed the regions of growth in the inner disk, it must dissipate a significant amount of angular momentum, about a factor of two or more within a dynamical time. It is not clear how it would accomplish this feat, as there are no signs of a bar or an intense interaction with a companion galaxy. Asymmetries in the mass distribution which would generate torques on the gas enabling the extended gas to dissipation energy and angular momentum are not readily apparent (e.g., Gavazzi et al. 2015). Given these circumstances, since a detailed analysis of this is beyond the scope of the paper, we simply raise the point that using the gas depletion time as an indicator of the duration of the star formation or its regulation is at best naive and at worst misleading. Higher resolution observations of the molecular gas might allow us to investigate this idea in more detail. Finally, we note that analysis by Spilker et al. (2015) shows that for a sample of distant galaxies with detection in the low-J CO lines, the CO emitting effective radii are larger than the effective radii of the star formation. Thus our claim that dynamical effects may be important in limiting the gas supply of galaxies could be generally true for the population of distant star-forming galaxies.

5.2. Previous detections of cold molecular gas in $z > 0.4$ cluster galaxies

Motivated by the CO(1−0) detection of the protocluster member HAE229, it is interesting to investigate the dependency of the physical properties of the molecular gas in (proto)cluster galaxies beyond $z \sim 0.4$, thus extending the previous study by Jablonka et al. (2013) of molecular gas in clusters members to higher redshifts. Therefore, we searched the literature for previous detections of cold molecular gas in (proto)cluster galaxies at $z > 0.4$. We restrict our search exclusively to CO(1−0) or CO(2−1) detections as we want robust estimates of the total amount of molecular gas masses (cf. Casey 2016). Using high-order CO transitions, from CO(3−2) upwards, can lead to significant underestimates of the true gas mass (e.g., Dannerbauer et al. 2009). High-order transitions trace the dense, high excitation gas closely associated with star-forming regions and feedback. The low-order transitions, CO(1−0) and CO(2−1)[6], trace the lower density gas, which is a better estimate of a galaxy's potential to form stars (e.g., Ivison et al. 2011; Emonts et al. 2015a). Including HAE229, we find 24 CO(1−0) and/or CO(2−1) bright

galaxies in 12 different galaxy overdensities beyond $z > 0.4$: seven lie between $0.4 < z < 1.0$, three between $1.0 < z < 2.0$, seven between $2.0 < z < 3.0$, one at $z = 3.1$, three at $z = 4$, and two beyond $z = 5$ (see Table A.1 for details). Our (proto)cluster sample is dominated by high-z sources (cf. Jablonka et al. 2013). The environments probed are both clusters and protoclusters at different evolutionary stages. The number of detections of cold molecular gas is still low compared to field galaxies and none of these clusters has a large number of detections. The infrared luminosity of this sample ranges between $L_{\rm IR} \sim 5-400 \times 10^{11}~L_{\odot}$. Based on this compilation, we conclude that even high $L'_{\rm CO}$ galaxies exist in high density fields (cf. Jablonka et al. 2013). Below $z = 1$ all of the cluster sources have a disk-like star-formation mode. Thus, we can extend the relation between $L_{\rm IR}$ and $L'_{\rm CO}$ for cluster galaxies both in $L_{\rm IR}$ and $L'_{\rm CO}$ compared to Jablonka et al. (2013) who were restricted up to $L_{\rm IR} < 10^{12}~L_{\odot}$ and $L'_{\rm CO} < 10^{10}$ K km s^{-1} pc^2. They concluded that the frequency of high $L'_{\rm CO}$ galaxies in clusters is lower than in the field implying that the molecular gas content of massive galaxies depends on environment.

With our compilation of 24 detections beyond $z > 0.4$, we find that above this redshift, as we now discuss, the cluster environment does not influence strongly the molecular gas content and other properties of galaxies in the early universe. We note that our sample at $z > 0.4$ is dominated by protoclusters members. Thus, there could be a bias in our compilation as high-z protocluster are, by definition, the early stages in the evolution of clusters (see Overzier 2016, for more details on protoclusters).

5.2.1. CO(1−0) line width-luminosity relation

The baryonic Tully-Fisher (T-F) relation can be understood as a natural relationship between angular momentum and mass of centrifugally-supported disk galaxies. In the standard cosmological model, a Tully-Fisher relationship results naturally if the fraction of the angular momentum and mass of the baryons are both fixed fractions of the angular momentum and mass of the dark matter halos themselves (Mo et al. 1998). The classical Tully-Fisher relationship is measured using the rotation speed of the disk and the total stellar content or luminosity of the disk or total baryonic mass (e.g., McGaugh & Schombert 2015). In a twist in the study of specific "T-F-like relations", Bothwell et al. (2013) found a relationship between CO luminosity, $L'_{\rm CO}$, and line width, FWHM, for SMGs (cf. Carilli & Walter 2013; Sharon et al. 2016). Goto & Toft (2015) confirm this finding. Bothwell et al. (2013) interpret this as a uniform ratio of the gas-to-stellar contribution to the dynamics of CO-bright regions. They model this trend as a relationship between the molecular gas mass and the velocity necessary for centrifugal support of a rotating disk. These authors further suggest that the low scatter, lower than that expected for randomly inclined disks, is due to the fact that galaxies at high redshift are geometrically thicker than their low redshift counterparts and that the molecular gas is a significant fraction of the total baryonic mass of the galaxies. Taking this relationship even further, despite its large scatter, Harris et al. (2012) and Zavala et al. (2015) use this relation to de-magnify (cf. Aravena et al. 2016) *Herschel*-selected lensed high-z galaxies (Negrello et al. 2010; Vieira et al. 2013; Messias et al. 2014).

Our discovery of a large rotating gas disk motivates us to investigate whether a Tully-Fisher relation exists for the CO emitting gas for a wider range of galaxies beyond just SMGs. Here we include high-z disk-like galaxies and search for

---

[6] We assume a ratio of 1 between the CO(2−1) and CO(1−0) luminosity.

differences between field and cluster galaxies. A difference is to be expected because additional processes operate in environments with higher galaxy and inter-galactic gas densities (e.g., Jablonka et al. 2013).

Our sample of (proto)cluster galaxies is a mix of disks and starbursts culled from the literature (see Table A.1). We find that most of the cluster sources beyond $z = 0.4$ follow the same L'_{CO}–FWHM relation as found for SMGs over the same redshift range (Bothwell et al. 2013; Goto & Toft 2015), but some of the galaxies in our sample lie below this relation (Fig. 7; see also Carilli & Walter 2013). Interestingly, the cluster galaxies below the relation are at low-z and overlap with the *Herschel* (ultra)-luminous infrared-galaxies ((U)LIRGs) field sample at intermediate redshifts (Magdis et al. 2014). In addition, we show unlensed, high-z field galaxies detected in CO(1−0) (Ivison et al. 2011; Bothwell et al. 2013) and normal star-forming galaxies selected via three color imaging (*B*-, *z*-, and *K*-band imaging – *BzK* galaxies; Daddi et al. 2004) that are detected in CO(1−0) and/or CO(2−1) (Daddi et al. 2008, 2010a; Aravena et al. 2010, 2014). Overall, we find that both normal SFGs and dusty starbursts at high-z follow the same relation as SMGs (Bothwell et al. 2013), while low- and intermediate-redshift ULIRGs perhaps have a weak trend offset from the high-z trend.

It is interesting that the SMGs and the disk galaxies in the field and protocluster environments appear to follow the same approximate relation. The explanation in Bothwell et al. (2013) of L'_{CO}–FWHM trend for distant galaxies is based on the argument that the galaxies in this relation are centrifugally-supported disks and the molecular gas constitutes a large fraction of the total mass. However, Bothwell et al. (2013) made two assumptions that may not be appropriate for all the galaxies on this relation. They assumed a conversion factor of 1 $M_\odot$ (K km s^{-1} pc^2)$^{-1}$ and a radius of 7 kpc to make the relation match the data. If the disks have a radius of a factor of 1.9 times higher than starbursts and a higher α_{CO} then the two relations, the ones for high and low redshift, would be the same. SMGs and normal SFGs may have the same parent population (e.g., Hayward et al. 2011, 2012; Béthermin et al. 2015), a finding that can perhaps be explained by a variation in the gas fraction: the gas fraction decreases with the total galaxy mass at a given redshift and decreases with decreasing redshift at a given total mass (e.g., Sargent et al. 2014). Since the baryons dominate the potential within the stellar mass distribution of halos, for a galaxy at a given baryonic mass (meaning constant FWHM if the gas motions are virialized), the gas fraction will decrease for galaxies with higher stellar mass (e.g., Sargent et al. 2014). Thus, we may expect the zero-point of the L'_{CO}–FWHM to decrease with decreasing redshift (if such a relation exists at all at lower redshifts).

The most interesting finding in this analysis, however, is not the significance of the trend, but that we do not find any difference between cluster and field galaxies in the FWHM–L'_{CO} plane for high-redshift sources. The trend is independent of the environment for the galaxies in these samples. This implies that for both field and (proto)cluster galaxies their gas content (gas as a total fraction of their total baryonic content) and dynamics are, within a wide scatter, similar. At lower redshifts, Jablonka et al. (2013) found that the field and cluster galaxies have different gas content for the equal stellar mass. This suggests that what ever processes dominate the regulation of the gas content of galaxies in low-redshift clusters do not operate as efficiently at redshifts ≳0.5−1.

However, intermediate-z sources do not follow this relation. Why? ULIRGs, the powerful infrared emitters at low and
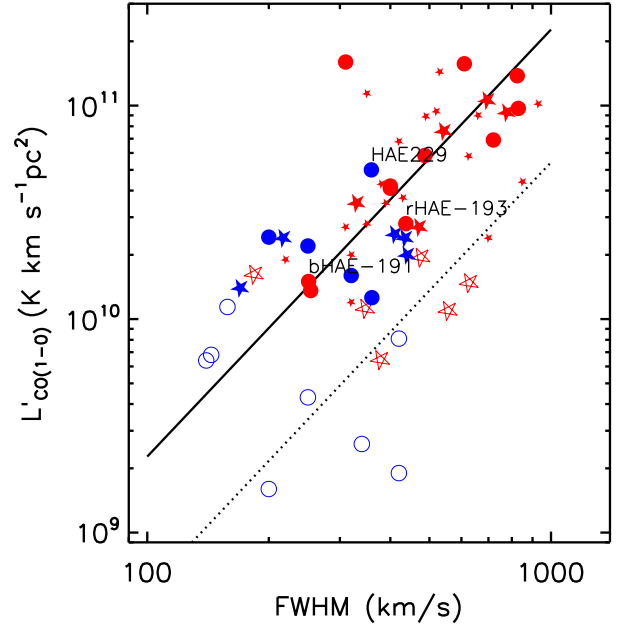
Fig. 7. Relation between FWHM of the CO(1−0) line and L'_{CO} for cluster (circles) and field galaxies (stars). High-redshift sources, those with $z > 1$, are indicated by filled symbols while sources with $z < 1$ are indicated by hollow ones. The color-coding used in the figure is as follows: intermediate-z ULIRGs (red hollow stars Magdis et al. 2014), normal SFGs at $z = 1.5$ (blue filled stars Daddi et al. 2010a; Aravena et al. 2014), and SMGs (large and small red filled stars from Ivison et al. 2011; Bothwell et al. 2013, respectively). References for cluster sources can be found in Sect. 5.2 and Table A.1. The mode of star formation for each source is color-coded as blue for "disk-like" and red for "starburst". The solid line shows the relation from Bothwell et al. (2013). The dashed line assumes the typical radius for disk galaxies. Both high-z population, dusty starbursts, and disk-like galaxies show a unique correlation between CO luminosity and line width with significant scatter (∼0.3 dex).

intermediate redshifts, are dominated by systems with strong random, non-virialized motions. Some SMGs, on the other hand, appear to have dynamics that are ordered, perhaps virialized (e.g., GN20; Hodge et al. 2012, 2013a) whether or not they lie in clustered environments. This agrees with the fact that SMGs are not simply scaled-up versions of local and intermediate-redshift ULIRGs (e.g., Swinbank et al. 2014).

5.2.2. Integrated Schmidt-Kennicutt relation

To further investigate whether or not being located in a galaxy overdensity has an impact on the gas content and star-formation rate of galaxies, we now study the relationship between star-formation rate and gas content – the integrated Schmidt-Kennicutt relation. The ratio of the SFR and M_{mol} can be thought of as a star-formation efficiency, that is, the conversion efficiency of gas into stars. We can cast this relationship directly between two observational quantities, one which is proportional to the SFR, the infrared luminosity, L_{IR}, and the other, to the mass of molecular gas, the CO luminosity, $L'_{CO(1-0)}$. If the conversion between L_{IR} and the SFR, and the conversion between $L'_{CO(1-0)}$ and the gas mass does not depend on the characteristics of the galaxies themselves, then this ratio, $L_{IR}/L'_{CO(1-0)}$, will be proportional to the "star-formation efficiency". Any differences found would then be attributable to the differences in the conversion between CO luminosity and the gas mass, $\alpha_{CO(1-0)}$, which would indicate that the excitation of the cold molecular gas depends on the

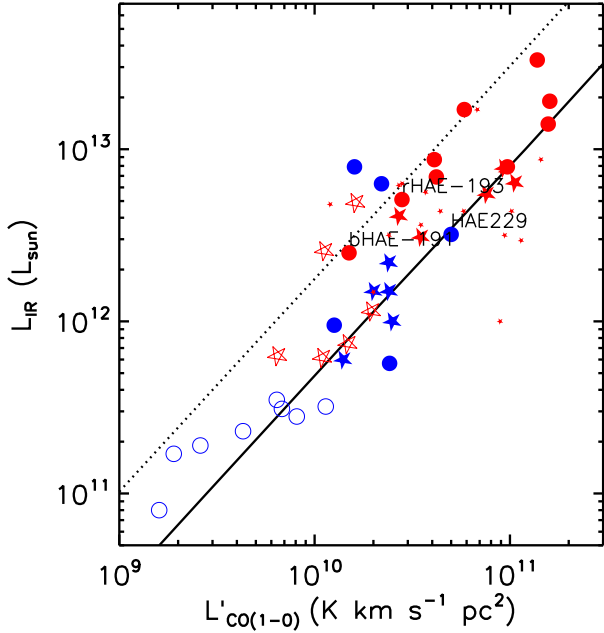**Fig. 8.** Relationship between L_{IR} and L'_{CO} – the integrated Schmidt-Kennicutt law – from our compilation of CO-bright galaxies lying in overdensities or protoclusters (circles, same encoding as in Fig. 7; Table A.1). The three CO-bright HAEs are indicated individually. HAE229 is clearly separated from the two other HAEs with CO detections (Tadaki et al. 2014), potentially indicating that red and blue HAEs have a wide range of CO luminosities. Small numbers of HAE with CO detections prohibit us from deciding if this is a real astrophysical effect. Solid and dashed lines are the best-fitting relations for normal star-forming and starburst galaxies (Sargent et al. 2014). At least within this small sample, no clear bi-modality in the star-formation efficiency is observed (cf. Daddi et al. 2010b; Genzel et al. 2010).

characteristics of the galaxies themselves. Alternatively, if there are not such dependencies in $\alpha_{CO(1-0)}$, any differences may be attributable to the rate at which gas is converted into stars, that is, the "star-formation efficiency".

Several studies have found a bi-modality in the integrated Schmidt-Kennicutt relation (e.g., Daddi et al. 2010b; Genzel et al. 2010). This bi-modality has been attributed to starburst galaxies having a higher star-formation efficiency than normal galaxies. This is despite having conversion factors that would suggest that starburst galaxies are less gas-rich in proportion to their CO luminosities. In Fig. 8, we investigate the L_{IR}/L'_{CO} ratio for our compiled CO-bright cluster sample, intermediate-z ULIRGs (Magdis et al. 2014), normal SFGs at $z = 1.5$ (Daddi et al. 2010a), and SMGs (Ivison et al. 2011; Bothwell et al. 2013)[7]. We find that HAE229 lies on the relation of disk-like galaxies whereas the other CO(1−0) detected HAEs (Tadaki et al. 2014) lie on the starburst relation (Sargent et al. 2014). At infrared luminosities below $L_{IR} = 2 \times 10^{12} L_\odot$, almost all galaxies follow the disk-like star-formation relation. Above this luminosity both relations, "disk-like" and "starburst", are populated. Interestingly, as previously pointed out, SMGs do not follow only the relation for ULIRGs and dusty starbursts but also lie at the region expected for disk-like galaxies (e.g., Swinbank et al. 2011; Hodge et al. 2012), demonstrating

---

[7] We note that in the absence of CO(1−0) observations, Bothwell et al. (2013) converted measurements of transitions higher than or equal to CO(2−1) into the CO(1−0) transition.

that this source population is not homogeneous (Hayward et al. 2011, 2012). Our analysis suggests that the simple dichotomy in the galaxy population based only on the star-formation efficiency is perhaps more complex than previous interpretations (e.g., Daddi et al. 2010b; Genzel et al. 2010). We do not find a difference of the L_{IR} and L'_{CO} relation between cluster and field galaxies. We therefore conclude, with the present data quality, that lying in a denser environment at high redshifts does not significantly alter the star-formation efficiency or the molecular gas excitation conditions in galaxies.

5.2.3. Are the environmental drivers of galaxy evolution efficient in the early Universe?

We have found that for gas-rich galaxies with redshifts larger than about 0.4, there does not appear to be an environmental dependence for the gas content, the star-formation efficiency, or on excitation conditions of the diffuse molecular gas as probed by low-order CO line transitions. This finding could be a sign that typical physical processes in local clusters that are responsible for depleting the content and altering the physical conditions of the gas in galaxies, like harassment, tidal stripping, and ram-pressure stripping (Moore et al. 1996; Vollmer et al. 2001b; Gnedin 2003a,b; Boselli & Gavazzi 2014) do not operate efficiently at high redshift (Jablonka et al. 2013; Husband et al. 2016). At higher redshift, for a given cluster mass, the internal galaxy-galaxy velocity dispersions of a protocluster will be higher than for local clusters. The galaxies surrounding the radio galaxy have extremely high relative projected velocities, of the order of 1000 km s^{-1}, suggesting that the protocluster is already massive (Kuiper et al. 2011). The processes that are likely to affect both the gas content and evolution of galaxies in clusters have very different dependences on the relative velocity of a galaxy as it moves through the population of cluster galaxies and cluster potential (e.g., Moore et al. 1996; Vollmer et al. 2001b; Gnedin 2003a,b). Both the harassment and tidal stripping rates are significantly lower if the galaxy, (1) has no close companions with small relative velocity; (2) has a high velocity relative to the mass center of the cluster; or (3) is not moving through regions of the cluster with a high galaxy volume density. In the case of HAE229, it has a high projected velocity relative to the radio galaxy which, if we assume it represents the center of mass of the cluster, implies that strong tidal stripping is very unlikely. It is also at a relatively large projected separation, about 250 kpc. While small compared to the likely virial radius of a massive dark matter halo at $z \sim 2$ (see Kuiper et al. 2011, and references therein), it means that HAE229 does not feel the influence of the total mass of the cluster. Also at high velocities, the timescale for harassment by other galaxies is very short and thus unlikely to be very effective in removing gas. These effects will be further reduced if protocluster galaxies have not yet virialized (Kuiper et al. 2011) and, at least in the case of HAE229, have yet to make their closest approach to the center of the protocluster potential.

However, the high velocity of HAE229 relative to the radio galaxy (~1200 km s^{-1}; Emonts et al. 2013) should, in principle, lead to very efficient ram pressure stripping. Ram pressure stripping is proportional to average gas volume density, $\langle \rho_w \rangle_v$ multiplied by the square of relative velocity of the galaxy in the potential, v_{rel}^2. The volume-averaged gas density is $\langle \rho_{gas} \rangle_v = \phi_{gas,v} \rho_{gas}$, where $\phi_{gas,v}$ is the gas volume-filling factor and ρ_{gas} is the density of the gas responsible for stripping the galaxy. The key to ram pressure operating effectively is for the gas within the cluster potential to have both a relatively high density and high filling

factor (e.g. Gnedin 2003b, models assume a high volume filling factor, $\phi_{gas,v} = 1$ for hot halo gas and thus neglect this term). The ram pressure must overcome the restoring force provided by the gravitation potential at the disk's surface. The higher velocities of galaxies in high-redshift (proto)clusters compared to low-redshift clusters[8], for a constant mass, suggest that the impact of ram pressure stripping should be enhanced, not diminished, in distant clusters. Gas at high temperatures dominate the intra-cluster medium (ICM) and the mass budget of low-redshift clusters (e.g., Laganá et al. 2013). The hot ICM gas has densities of $\sim 10^{-3}$ to 10^{-1} cm^{-3}, temperatures of $\sim 10^7$ to 10^8 K, and a near unity filling factor (e.g., Sanderson et al. 2009). The densities, unity filling factor, and high velocity dispersion of the galaxies is why ram pressure stripping is so effective in low-redshift clusters (e.g., Vollmer et al. 2001a,b; Fumagalli et al. 2014; Boselli et al. 2014, 2016). The near unity filling factor of the hot gas means that, as the galaxy is moving through the ICM, it feels a steady wind of material with slowly varying density depending on where it is relative to the cluster center. Since we do not find a strong impact on the gas content like that seen in local cluster galaxies, it must be that the dominant gas phase in distant protoclusters either has a density which is much less but still has a filling factor of unity, or that it has a much lower volume filling factor than in local clusters.

The ram pressure due to the ICM is counterbalanced by the restorative force of the disk's gravitational potential. The restorative force is proportion to the radial distribution of the combined stellar and gaseous surface mass density. In other words, galaxies with compact and roughly equal gaseous and stellar mass surface densities have maximal restoring forces and are resistant to ram pressure stripping. But galaxies at high redshift, and HAE229 in particular, have very extended gas distributions. The disk of HAE229 extends well beyond its stellar light. We would expect its outer gas disk to be easily stripped. For that matter, even tidal stripping should be effective in such extended disks. Why has HAE229 not been stripped? Again, this would be consistent with the mass content of the IGM of high-redshift clusters not having a high-volume filling factor gas of sufficient volume-weighted density. While we use the detailed properties of HAE229 to investigate the impact of environmental processes on the gas properties of galaxies, Figs. 7 and 8 suggest that HAE229, at least within this context, is not unusual or special.

While it is beyond the scope of this paper to quantitatively constrain the characteristics of the ICM in high-redshift protoclusters, there are a number of studies of how the ICM may develop. What we are suggesting here is that the mass distribution of the (proto)ICM at high redshift contains a significant fraction of low volume filling factor warm, $\sim 10^4$ K, and cold, ~ 10 K, gas. Accreting gas into massive halos alone does not explain the entropy profiles of the ICM of local clusters, even in the absence of cooling (e.g., Voit et al. 2005). It is clear that feedback from active galactic nuclei and star formation in cluster galaxies is necessary to provide sufficient entropy and heating to globally balance the cooling (Best et al. 2006). However, the energy and momentum injection from AGN, such as from the radio galaxy MRC 1138−262, is perhaps heating the

gas, but also induces substantial cooling and dissipation (e.g., Emonts et al. 2014, 2015b, 2016; Voit et al. 2015; Meece et al. 2015; Gullberg et al. 2016). Specifically, the large scale environment of MRC 1138−262 has a substantial Lyα emitting halo (Pentericci et al. 1997) and a significant mass of cold molecular gas (Emonts et al. 2016). Despite it being likely to have relatively high densities, $\sim 0.01-1$ cm^{-3} and $\sim 100-1000$ cm^{-3}, the volume filling factors of both these phases are undoubtedly minuscule ($\ll 0.1$). Instead of being a continuous wind of low density hot gas as in local clusters, these would be more like an intermittent shotgun blast of cold dense clouds. Under such circumstances the concept of ram pressure is completely inappropriate. The ISM of the galaxy does not feel a constant force of the fluid as is assumed in the relation between ram pressure and the gravitational restoring force (Gunn & Gott 1972). There of course could still be a diffuse high-volume filling factor hot gas, but its density must be substantially lower than that in local clusters (Carilli et al. 2002). More work theoretically and observationally is needed to understand our results (Emonts et al. 2016), but the very extended CO disk of HAE229 is already yielding fascinating clues as to the structure of early intra-cluster media in protoclusters.

6. Conclusion

We have presented the most detailed CO(1−0) observations to date for a distant, $z_{CO} = 2.1478$, normal star-forming galaxy. We detect the cold molecular gas reservoir of the Hα emitter #229 in very deep observations with the ATCA. Interestingly, a significant fraction of the CO emission lies outside the rest-frame UV/optical emitting galaxy. The physical properties of HAE229 indicate that this source lies on the main sequence of galaxies and its relatively long gas depletion time and disk morphology suggest that it is the first CO(1−0)-bright HAE with a "quiescent mode" of star-formation.

In order to study the environmental dependency of the gas fraction at high redshifts, we compiled a sample of 24 high-z (proto)cluster members from the literature. We do not find any environmental dependence suggesting that usual physical processes seen in local clusters such as harassment, tidal stripping, and ram-pressure stripping do not operate efficiently at high redshift in over-dense environments.

In addition, we extend the relation between L'_{CO} and FWHM of the CO line previously valid for starbursts (Bothwell et al. 2013) to gas-rich main-sequence galaxies beyond $z = 1$. Our analysis of the integrated Schmidt-Kennicutt law indicates that the proposed dichotomy between starbursts and disk galaxies is perhaps more complex than known heretofore.

Finally, we stress that the number of CO detections of (proto)cluster galaxies in the distant universe is still very low compared to field galaxies. In order to understand the influence of the environment on the molecular gas reservoirs and star-formation efficiency, systematic surveys of (proto)cluster galaxies beyond $z = 1$ in low-order CO lines must be conducted.

---

[8] The cluster velocity dispersion, σ, scales as the virial velocity, $(GM_v/r_v)^{1/2}$, where M_v and r_v are the virial mass and radius, respectively. This relation scales as $(\Delta(z)/2)^{1/6} (GH(z) M_v)^{1/3}$, where the mean density of the halo is $\Delta(z)$ halo times the critical density, $H(z)$ is the Hubble constant, and G is the gravitational constant. $\Delta(z)$ increases slowly with increasing z, the Hubble constant $H(z)$ increases rapidly with z, and thus so does the velocity of galaxies in halos of constant virial mass as a function of redshift.

References

Abraham, R. G., van den Bergh, S., & Nair, P. 2003, ApJ, 588, 218
Aravena, M., Carilli, C., Daddi, E., et al. 2010, ApJ, 718, 177
Aravena, M., Carilli, C. L., Salvato, M., et al. 2012, MNRAS, 426, 258
Aravena, M., Hodge, J. A., Wagg, J., et al. 2014, MNRAS, 442, 558
Aravena, M., Spilker, J. S., Bethermin, M., et al. 2016, MNRAS, 457, 4406
Baker, A. J., Tacconi, L. J., Genzel, R., Lehnert, M. D., & Lutz, D. 2004, ApJ, 604, 125
Best, P. N., Kaiser, C. R., Heckman, T. M., & Kauffmann, G. 2006, MNRAS, 368, L67
Béthermin, M., Daddi, E., Magdis, G., et al. 2015, A&A, 573, A113
Béthermin, M., De Breuck, C., Gullberg, B., et al. 2016, A&A, 586, L7
Bigiel, F., Leroy, A., Walter, F., et al. 2008, AJ, 136, 2846
Blain, A. W., Smail, I., Ivison, R. J., Kneib, J.-P., & Frayer, D. T. 2002, Phys. Rep., 369, 111
Bolatto, A. D., Wolfire, M., & Leroy, A. K. 2013, ARA&A, 51, 207
Boselli, A., & Gavazzi, G. 2014, A&ARv, 22, 74
Boselli, A., Voyer, E., Boissier, S., et al. 2014, A&A, 570, A69
Boselli, A., Cuillandre, J. C., Fossati, M., et al. 2016, A&A, 587, A68
Bothwell, M. S., Smail, I., Chapman, S. C., et al. 2013, MNRAS, 429, 3047
Briggs, D. S. 1995, Ph.D. Thesis, New Mexico Institute of Mining and Technology
Cañameras, R., Nesvadba, N. P. H., Guery, D., et al. 2015, A&A, 581, A105
Capak, P. L., Riechers, D., Scoville, N. Z., et al. 2011, Nature, 470, 233
Carilli, C. L., & Walter, F. 2013, ARA&A, 51, 105
Carilli, C. L., Harris, D. E., Pentericci, L., et al. 2002, ApJ, 567, 781
Casey, C. M. 2012, MNRAS, 425, 3094
Casey, C. M. 2016, ApJ, 824, 36
Casey, C. M., Narayanan, D., & Cooray, A. 2014, Phys. Rep., 541, 45
Casasola, V., Magrini, L., Combes, F., et al. 2013, A&A, 558, A60
Chabrier, G. 2003, PASP, 115, 763
Chamaraux, P., Balkowski, C., & Gerard, E. 1980, A&A, 83, 38
Chamaraux, P., Balkowski, C., & Fontanelli, P. 1986, A&A, 165, 15
Chapman, S. C., Bertoldi, F., Smail, I., et al. 2015, MNRAS, 453, 951
Daddi, E., Cimatti, A., Renzini, A., et al. 2004, ApJ, 617, 746
Daddi, E., Dickinson, M., Morrison, G., et al. 2007, ApJ, 670, 156
Daddi, E., Dannerbauer, H., Elbaz, D., et al. 2008, ApJ, 673, L21
Daddi, E., Dannerbauer, H., Stern, D., et al. 2009, ApJ, 694, 1517
Daddi, E., Bournaud, F., Walter, F., et al. 2010a, ApJ, 713, 686
Daddi, E., Elbaz, D., Walter, F., et al. 2010b, ApJ, 714, L118
Daddi, E., Dannerbauer, H., Liu, D., et al. 2015, A&A, 577, A46
Dannerbauer, H., Daddi, E., Riechers, D. A., et al. 2009, ApJ, 698, L178
Dannerbauer, H., Kurk, J. D., De Breuck, C., et al. 2014, A&A, 570, A55
Denicoló, G., Terlevich, R., & Terlevich, E. 2002, MNRAS, 330, 69
Doherty, M., Tanaka, M., De Breuck, C., et al. 2010, A&A, 509, A83
Draine, B. T., & Li, A. 2007, ApJ, 657, 810
Dye, S., Furlanetto, C., Swinbank, A. M., et al. 2015, MNRAS, 452, 2258
Emonts, B. H. C., Norris, R. P., Feain, I., et al. 2011, MNRAS, 415, 655
Emonts, B. H. C., Feain, I., Röttgering, H. J. A., et al. 2013, MNRAS, 430, 3465
Emonts, B. H. C., Norris, R. P., Feain, I., et al. 2014, MNRAS, 438, 2898
Emonts, B. H. C., De Breuck, C., Lehnert, M. D., et al. 2015a, A&A, 584, A99
Emonts, B. H. C., Mao, M. Y., Stroe, A., et al. 2015b, MNRAS, 451, 1025
Emonts, B. H. C., Lehnert, M. D., Villar-Martín, M., et al. 2016, Science, 354, 1128
Fumagalli, M., Fossati, M., Hau, G. K. T., et al. 2014, MNRAS, 445, 4335
Gavazzi, G., Consolandi, G., Dotti, M., et al. 2015, A&A, 580, A116
Geach, J. E., Smail, I., Coppin, K., et al. 2009, MNRAS, 395, L62
Geach, J. E., Smail, I., Moran, S. M., et al. 2011, ApJ, 730, L19

Genzel, R., Tacconi, L. J., Gracia-Carpio, J., et al. 2010, MNRAS, 407, 2091
Genzel, R., Tacconi, L. J., Lutz, D., et al. 2015, ApJ, 800, 20
Gnedin, O. Y. 2003a, ApJ, 582, 141
Gnedin, O. Y. 2003b, ApJ, 589, 752
Gooch, R. 1996, in Astronomical Data Analysis Software and Systems V, eds. G. H. Jacoby, & J. Barnes, ASP Conf. Ser., 101, 80
Goto, T., & Toft, S. 2015, A&A, 579, A17
Greve, T. R., Bertoldi, F., Smail, I., et al. 2005, MNRAS, 359, 1165
Gullberg, B., Lehnert, M. D., De Breuck, C., et al. 2016, A&A, 591, A73
Gunn, J. E., & Gott, J. R., III 1972, ApJ, 176, 1
Hatch, N. A., Kurk, J. D., Pentericci, L., et al. 2011, MNRAS, 415, 2993
Harrington, K. C., Yun, M. S., Cybulski, R., et al. 2016, MNRAS, 458, 4383
Harris, A. I., Baker, A. J., Frayer, D. T., et al. 2012, ApJ, 752, 152
Hayward, C. C., Kereš, D., Jonsson, P., et al. 2011, ApJ, 743, 159
Hayward, C. C., Jonsson, P., Kereš, D., et al. 2012, MNRAS, 424, 951
Hodge, J. A., Carilli, C. L., Walter, F., et al. 2012, ApJ, 760, 11
Hodge, J. A., Karim, A., Smail, I., et al. 2013a, ApJ, 768, 91
Hodge, J. A., Carilli, C. L., Walter, F., Daddi, E., & Riechers, D. 2013b, ApJ, 776, 22
Husband, K., Bremer, M. N., Stott, J. P., & Murphy, D. N. A. 2016, MNRAS, 462, 421
Ilbert, O., McCracken, H. J., Le Fèvre, O., et al. 2013, A&A, 556, A55
Ivison, R. J., Morrison, G. E., Biggs, A. D., et al. 2008, MNRAS, 390, 1117
Ivison, R. J., Papadopoulos, P. P., Smail, I., et al. 2011, MNRAS, 412, 1913
Ivison, R. J., Smail, I., Amblard, A., et al. 2012, MNRAS, 425, 1320
Ivison, R. J., Swinbank, A. M., Smail, I., et al. 2013, ApJ, 772, 137
Jablonka, P., Combes, F., Rines, K., Finn, R., & Welch, T. 2013, A&A, 557, A103
Karim, A., Swinbank, M., Hodge, J., et al. 2013, MNRAS, 432, 2
Koyama, Y., Kodama, T., Tadaki, K.-i., et al. 2013, MNRAS, 428, 1551
Kuiper, E., Hatch, N. A., Miley, G. K., et al. 2011, MNRAS, 415, 2245
Kurk, J. D., Röttgering, H. J. A., Pentericci, L., et al. 2000, A&A, 358, L1
Kurk, J. D., Pentericci, L., Röttgering, H. J. A., & Miley, G. K. 2004a, A&A, 428, 793
Kurk, J. D., Pentericci, L., Overzier, R. A., Röttgering, H. J. A., & Miley, G. K. 2004b, A&A, 428, 817
Laganá, T. F., Martinet, N., Durret, F., et al. 2013, A&A, 555, A66
Lehnert, M. D., van Driel, W., Le Tiran, L., Di Matteo, P., & Haywood, M. 2015, A&A, 577, A112
Leroy, A. K., Walter, F., Brinks, E., et al. 2008, AJ, 136, 2782
Leroy, A. K., Bolatto, A., Gordon, K., et al. 2011, ApJ, 737, 12
Lestrade, J.-F., Combes, F., Salomé, P., et al. 2010, A&A, 522, L4
Magdis, G. E., Daddi, E., Elbaz, D., et al. 2011, ApJ, 740, L15
Magdis, G. E., Daddi, E., Béthermin, M., et al. 2012, ApJ, 760, 6
Magdis, G. E., Rigopoulou, D., Hopwood, R., et al. 2014, ApJ, 796, 63
Maier, C., Lilly, S. J., Ziegler, B. L., et al. 2014, ApJ, 792, 3
Mannucci, F., Cresci, G., Maiolino, R., Marconi, A., & Gnerucci, A. 2010, MNRAS, 408, 2115
McGaugh, S. S., & Schombert, J. M. 2015, ApJ, 802, 18
Meece, G. R., O'Shea, B. W., & Voit, G. M. 2015, ApJ, 808, 43
Messias, H., Dye, S., Nagar, N., et al. 2014, A&A, 568, A92
Michałowski, M. J., Watson, D., & Hjorth, J. 2010, ApJ, 712, 942
Miley, G. K., Overzier, R. A., Zirm, A. W., et al. 2006, ApJ, 650, L29
Mo, H. J., Mao, S., & White, S. D. M. 1998, MNRAS, 295, 319
Moore, B., Katz, N., Lake, G., Dressler, A., & Oemler, A. 1996, Nature, 379, 613
Narayanan, D., Turk, M., Feldmann, R., et al. 2015, Nature, 525, 496
Negrello, M., Hopwood, R., De Zotti, G., et al. 2010, Science, 330, 800
Ogle, P., Davies, J. E., Appleton, P. N., et al. 2012, ApJ, 751, 13
Oke, J. B., & Gunn, J. E. 1983, ApJ, 266, 713
Overzier, R. A. 2016, A&ARv, 24, 14
Pannella, M., Carilli, C. L., Daddi, E., et al. 2009, ApJ, 698, L116
Papadopoulos, P. P., Feain, I. J., Wagg, J., & Wilner, D. J. 2008, ApJ, 684, 845
Pentericci, L., Roettgering, H. J. A., Miley, G. K., Carilli, C. L., & McCarthy, P. 1997, A&A, 326, 580
Pentericci, L., Kurk, J. D., Röttgering, H. J. A., et al. 2000, A&A, 361, L25
Pettini, M., & Pagel, B. E. J. 2004, MNRAS, 348, L59
Pope, A., Chary, R.-R., Alexander, D. M., et al. 2008, ApJ, 675, 1171
Riechers, D. A., Capak, P. L., Carilli, C. L., et al. 2010, ApJ, 720, L131
Riechers, D. A., Carilli, C. L., Walter, F., et al. 2011, ApJ, 733, L11
Rodighiero, G., Daddi, E., Baronchelli, I., et al. 2011, ApJ, 739, L40
Salpeter, E. E. 1955, ApJ, 121, 161
Sanderson, A. J. R., O'Sullivan, E., & Ponman, T. J. 2009, MNRAS, 395, 764
Sargent, M. T., Daddi, E., Béthermin, M., et al. 2014, ApJ, 793, 19
Sault, R. J., Teuben, P. J., & Wright, M. C. H. 1995, Astronomical Data Analysis Software and Systems IV, 77, 433
Scoville, N., Sheth, K., Aussel, H., et al. 2016, ApJ, 820, 83
Sharon, C. E., Riechers, D. A., Hodge, J., et al. 2016, ApJ, 827, 18

Smail, I., Swinbank, A. M., Ivison, R. J., & Ibar, E. 2011, MNRAS, 414, L95
Solomon, P. M., & Vanden Bout, P. A. 2005, ARA&A, 43, 677
Spergel, D. N., Verde, L., Peiris, H. V., et al. 2003, ApJS, 148, 175
Spergel, D. N., Bean, R., Doré, O., et al. 2007, ApJS, 170, 377
Spilker, J. S., Marrone, D. P., Aguirre, J. E., et al. 2014, ApJ, 785, 149
Spilker, J. S., Aravena, M., Marrone, D. P., et al. 2015, ApJ, 811, 124
Stevens, J. A., Ivison, R. J., Dunlop, J. S., et al. 2003, Nature, 425, 264
Swinbank, A. M., Chapman, S. C., Smail, I., et al. 2006, MNRAS, 371, 465
Swinbank, A. M., Papadopoulos, P. P., Cox, P., et al. 2011, ApJ, 742, 11
Swinbank, A. M., Simpson, J. M., Smail, I., et al. 2014, MNRAS, 438, 1267
Swinbank, A. M., Dye, S., Nightingale, J. W., et al. 2015, ApJ, 806, L17
Tacconi, L. J., Genzel, R., Smail, I., et al. 2008, ApJ, 680, 246
Tacconi, L. J., Genzel, R., Neri, R., et al. 2010, Nature, 463, 781
Tacconi, L. J., Neri, R., Genzel, R., et al. 2013, ApJ, 768, 74
Tadaki, K.-i., Kodama, T., Tamura, Y., et al. 2014, ApJ, 788, 23
Tanaka, M., De Breuck, C., Venemans, B., & Kurk, J. 2010, A&A, 518, A18

Tan, Q., Daddi, E., Magdis, G., et al. 2014, A&A, 569, A98
Vandame, B. 2004, Ph.D. Thesis, Nice University, France
Vieira, J. D., Marrone, D. P., Chapman, S. C., et al. 2013, Nature, 495, 344
Voit, G. M., Kay, S. T., & Bryan, G. L. 2005, MNRAS, 364, 909
Voit, G. M., Donahue, M., Bryan, G. L., & McDonald, M. 2015, Nature, 519, 203
Vollmer, B., Cayatte, V., van Driel, W., et al. 2001a, A&A, 369, 432
Vollmer, B., Cayatte, V., Balkowski, C., & Duschl, W. J. 2001b, ApJ, 561, 708
Wagg, J., Pope, A., Alberts, S., et al. 2012, ApJ, 752, 91
Wang, T., Elbaz, D., Daddi, E., et al. 2016, ApJ, 828, 56
Walter, F., Carilli, C., Bertoldi, F., et al. 2004, ApJ, 615, L17
Walter, F., Decarli, R., Carilli, C., et al. 2012, Nature, 486, 233
Weiß, A., Kovács, A., Coppin, K., et al. 2009, ApJ, 707, 1201
Weiß, A., De Breuck, C., Marrone, D. P., et al. 2013, ApJ, 767, 88
Zavala, J. A., Yun, M. S., Aretxaga, I., et al. 2015, MNRAS, 452, 1140
Zirm, A. W., Stanford, S. A., Postman, M., et al. 2008, ApJ, 680, 224

Appendix A: Properties of distant galaxies in overdensities

Table A.1. CO observations of $z > 0.4$ cluster members.

Name	z_{CO}	Transition	I_{CO} (Jy km^{-1})	$FWHM$ (km s^{-1})	Telescope	L'_{CO} (10^{10} K km s^{-1} pc^2)	L_{IR} (10^{12} $L_\odot$)	Reference
Cluster Cl0024+16 at z = 0.40								
MIPS J002652.5	0.3799	1−0		140 ± 10	PdBI	0.64 ± 0.05	3.5 ± 0.5	Geach et al. (2011)
MIPS J002621.7	0.3803	1−0		144 ± 14	PdBI	0.68 ± 0.06	3.1 ± 0.2	Geach et al. (2009)
MIPS J002715.0	0.3813	1−0		340 ± 40	PdBI	0.26 ± 0.03	1.9 ± 0.3	Geach et al. (2011)
MIPS J002703.6	0.3956	1−0		250 ± 30	PdBI	0.43 ± 0.06	2.3 ± 0.3	Geach et al. (2011)
MIPS J002721.0	0.3964	1−0		158 ± 34	PdBI	1.14 ± 0.11	3.2 ± 0.2	Geach et al. (2009)
Cluster Cl1416+4446 at z = 0.40								
GAL1416+446	0.3964	1−0	1.0 ± 0.1	420 ± 40	PdBI	0.81 ± 0.8	0.275	Jablonka et al. (2013)
Cluster Cl09266+1242 at z = 0.49								
GAL0926+1242−A	0.4886	2−1	0.6 ± 0.1	420 ± 40	PdBI	0.19 ± 0.03	0.165	Jablonka et al. (2013)
GAL0926+1242−B	0.4886	2−1	0.5 ± 0.1	200 ± 20	PdBI	0.16 ± 0.03	0.082	Jablonka et al. (2013)
Cluster 7C 1756+6520 at z = 1.42								
AGN.1317	1.4161 ± 0.0001	2−1	0.52 ± 0.06	254 ± 33	PdBI	1.36 ± 0.15		Casasola et al. (2013)
Cluster COSMOS at z = 1.55								
51613	1.517	1−0	0.20 ± 0.05	200 ± 80	VLA	2.42 ± 0.58	0.57	Aravena et al. (2012)
51858	1.556	1−0	0.10 ± 0.03	360 ± 220	VLA	1.26 ± 0.38	0.95	Aravena et al. (2012)
Protocluster MRC 1138−262 at z = 2.16								
HAE229	2.1480 ± 0.0004	1−0	0.22 ± 0.03	359 ± 34	ATCA	5.0 ± 0.7	3.2	this paper
Protocluster HATLAS J084933 at z = 2.41								
HATLAS J084933 W	2.4066 ± 0.0006	1−0	0.49 ± 0.06	825 ± 115	VLA	13.8 ± 1.7	$33.1^{+3.2}_{-2.9}$	Ivison et al. (2013)
HATLAS J084933 T	2.4090 ± 0.0003	1−0	0.56 ± 0.07	610 ± 55	VLA	15.7 ± 2.0	$14.5^{+1.8}_{-1.6}$	Ivison et al. (2013)
HATLAS J084933 M	2.4176 ± 0.0004	1−0	0.057 ± 0.013	320 ± 70	VLA	1.6 ± 0.4	$7.9^{+4.6}_{-2.9}$	Ivison et al. (2013)
HATLAS J084933 C	2.4138 ± 0.0003	1−0	0.079 ± 0.014	250 ± 100	VLA	2.2 ± 0.4	$6.3^{+3.7}_{-2.3}$	Ivison et al. (2013)
Protocluster USS 1558−003 at z = 2.51								
rHAE−193	2.5131	1−0	0.096 ± 0.015	437	VLA	2.8	5.1	Tadaki et al. (2014)
bHAE−191	2.5168	1−0	0.052 ± 0.008	251	VLA	1.5	2.5	Tadaki et al. (2014)
Protocluster B3 J2330 at z = 3.09								
JVLA J233024.69+392708.6	3.0884 ± 0.0010	1−0	0.16 ± 0.03	720 ± 170	VLA	6.9 ± 1.5		Ivison et al. (2012)
Protocluster GN20 at z = 4.05								
GN20	4.0548 ± 0.0008	2−1	1.0 ± 0.3	310 ± 110	VLA	16.0 ± 5.0	$18.6^{+0.9}_{-0.8}$	Hodge et al. (2012), Tan et al. (2014)
GN20.2a	4.051 ± 0.001	2−1	0.6 ± 0.2	830 ± 190	VLA	9.7 ± 2.9	$7.9^{+0.4}_{-0.9}$	Hodge et al. (2013a), Tan et al. (2014)
GN20.2b	4.056 ± 0.001	2−1	0.3 ± 0.2	400 ± 210	VLA	4.2 ± 2.9	$6.9^{+0.7}_{-1.4}$	Hodge et al. (2013a), Tan et al. (2014)
Protocluster HDF850.1 at z = 5.18								
HDF850.1	5.183	2−1	0.17 ± 0.04	400 ± 30	VLA	4.1	8.7 ± 1.0	Walter et al. (2012)
Protocluster AzTEC-3 at z = 5.30								
AzTEC−3	5.2979 ± 0.0004	2−1	0.23 ± 0.03	487 ± 58	VLA	5.84 ± 0.78	17 ± 8	Riechers et al. (2010)